Journal of Marine Science and Technology

Volume 28 | Issue 6 Article 9

A New Complex Marine Unmanned Platform and Field Test

Jihyeong Lee
Department of Mechanical Engineering, Korea Maritime and Ocean University, Busan, Korea

Han-Sol Jin
Department of Mechanical Engineering, Korea Maritime and Ocean University, Busan, Korea

Hyunjoon Cho
Department of Mechanical Engineering, Korea Maritime and Ocean University, Busan, Korea

Jiafeng Huang
Department of Mechanical Engineering, Korea Maritime and Ocean University, Busan, Korea

Sang-Ki Jeong
Maritime ICT R&D Center, Korea Institute of Ocean Science & Technology, Busan, Korea

See next page for additional authors

A New Complex Marine Unmanned Platform and Field Test

Acknowledgements

This research was supported by “Data Collection System with Underwater Glider (19AR0001)” funded by Agency for Defense Development, Korea.

Authors

Jihyeong Lee, Han-Sol Jin, Hyunjoon Cho, Jiafeng Huang, Sang-Ki Jeong, Dae-Hyeong Ji, and Hyeung-Sik Choi

Journal of Marine Science and Technology, Vol. 28, No. 6, pp. 538-547 (2020)
DOI: 10.6119/JMST.202012_28(6).0009

A NEW COMPLEX MARINE UNMANNED PLATFORM AND FIELD TEST

Jihyeong Lee[1], Han-Sol Jin[1], Hyunjoon Cho[1], Huang Jiafeng[1] , Sang-Ki Jeong[2], Dae-Hyeong Ji[3] and Hyeung-Sik Choi[1]

Key words: unmanned surface vehicle, unmanned underwater vehicle, complex marine unmanned platform, dynamic positioning.

ABSTRACT

This paper presents the development of a new complex marine unmanned platform composed of an unmanned surface vehicle (USV) and a remotely operated vehicle (ROV), and the results of a sea test. The platform structure, control system, sensor system, and control algorithm were developed and are introduced. The complex platform collects information of the underwater structures, such as the wall, floor, and piers and harbors. Using a tether cable, the ROV is connected to the USV for power supply and to receive a large amount of underwater data obtained using a sonar scanner or a camera in real time. The ultra-short baseline transponder is attached to the USV hull to determine the position of the ROV in real time where a transponder is installed. The ROV can be launched and recovered using the winch system installed on the USV. The data collected by the two vehicles can be transmitted to an operating center in real time via radio frequency (RF) communications.

A new CTE tracking algorithm and a dynamic positioning algorithm are proposed. The proposed algorithms are implemented by conducting sea tests, and the results of the performance tests are presented. In particular, for the hovering control of the ROV, a proportional–integral–differential (PID) controller and a robust sliding mode control (SMC) are applied, and the superior performance of the SMC is presented.

Paper submitted 06/01/20; revised 09/21/20; accepted 12/01/20. Corresponding Author: Hyeung-Sik Choi (e-mail:hchoi@kmou.ac.kr)

[1] Department of Mechanical Engineering, Korea Maritime and Ocean University, Busan, Korea
[2] Maritime ICT R&D Center, Korea Institute of Ocean Science & Technology, Busan, Korea
[3] Marine Security and Safety Research Center, Korea Institute of Ocean Science & Technology, Busan, Korea

I. INTRODUCTION

The importance of various resources, such as oil, gas, and rare earth elements, is increasingly highlighting the need to develop marine exploration vehicles, and in particular, the unmanned exploration vehicles due to safety and cost issues (Bentley, 2002; Nicholson and Healey, 2008). Currently, most construction or maintenance works of offshore structures involve divers entering and working directly in the ocean (Kim et al., 2015). However, it is difficult for humans to dive to a depth of 30 m or deeper, or to continue working underwater for more than an hour. Therefore, several research are being conducted on the subject of unmanned surface vehicles (USVs) and the utilization of unmanned underwater vehicles (UUVs) in relation to USVs (Chen et al., 2019; Rodriguez et al., 2019). Among underwater robots, remotely operated vehicles (ROVs) have the advantage of being able to secure location data through GPS because they are operated from the mother ship, being unrestricted in terms of operating time due to energy limitations, and receiving underwater data in real time. However, the disadvantages are that the tether cable connecting the mother ship and the ROV constrains the radius of action; therefore, it needs to be operated by a trained operator due to difficulties in handling (Cho et al., 2020). In 2018, Lachaud et al. proposed a combined USV–ROV and conducted a communication analysis between the USV and ROV (Lachaud et al., 2018). However, it does not have a coordination system between the USV and ROV (Lyu et al., 2018). In addition, mathematical modeling for the complex platform and the underwater cable drag analysis were presented without an actual platform or field test results (Vu. et al., 2020). Recently, commercial platforms combining underwater and water surface platforms capable of acquiring real-time data using an underwater cable have appeared, but without detailed information on performance (BORSYS, 2019; CAT-Surveyor, 2020). Therefore, in this study, the advantages of USV and ROV are combined to create a platform in which USVs and ROVs can perform a task on the coast where a large work vessel is difficult to approach, and to fur ROV. The complex platform is usually affected by the tether cable connecting the USV and ROV (Vu. et al., 2017; Vu. et

al., 2020). Because the complex platform developed in this study was placed on the coast at a shallow depth, the effect of the cable was not taken into consideration. A catamaran-form USV hull was selected due to its excellent rolling, resilience, and linear motion properties suitable for marine exploration (Molland et al., 1994). Furthermore, the tether cable provided a stable power supply to the ROV and real-time underwater data. The structure and control system of the complex platform developed in this study were designed and fabricated for long-term operation, real-time underwater data collection, and relative position measurement using GPS and ultra-short baseline (USBL).

II. SYSTEM STRUCTURE OF COMPLEX PLATFORM

1.System Structure of USV

The USV developed in this study consists of a hull, a thruster, a control system, a communication system, and a winch system. Fig. 1 and Table 1 show the specifications and configuration of the USV, respectively. Synthetic rubber materials are used for hulls because of their advantages such as water resistance, corrosion resistance, and prevention of damage to the hull during collision. The USV is equipped with a battery pack of 24 V for power supply to the system, a battery pack of 48 V for power supply to the ROV system, a control box, and a winch system. A camera and a LiDAR sensor are installed to detect obstacles in the front and to check the operation route of the USV. A winch system is installed to connect the USV to the ROV, supply power to the ROV, transmit and receive data, and control the ROV depth for underwater exploration.

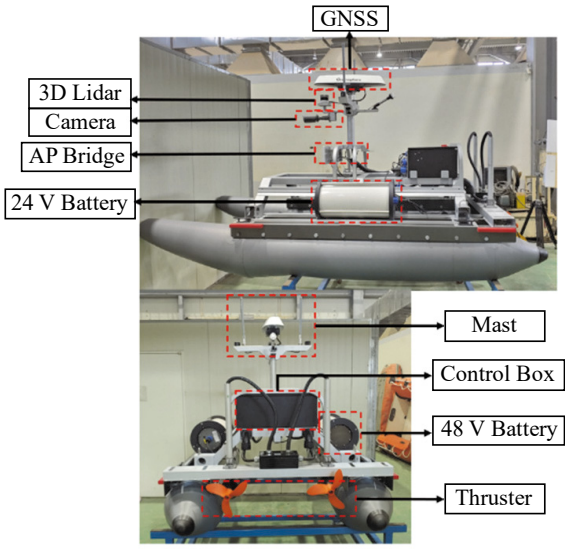

Fig. 1. Configuration of USV

Table 1. Specifications of USV

Size (L *W * H) (mm)	3250*1500*1860
Weight (kg)	153.5
GNSS	Hemisphere Vector V113
Battery	24V 160Ah, 48V 80Ah
USBL	Blueprint Subsea SeaTrac X150, X010
Main Controller	MSI cubi 3 silent
AP Bridge	GT-Wave 860S
Thruster	Torqeedo Cruise 2.0T

2. System Structure of ROV

The ROV is designed to explore underwater structures or sea level. It is usually docked with the USV, and uses the winch system of the USV to go underwater and perform tasks when it reaches the task position. The main sensors mounted on the ROV for the exploration are a tilt camera, 360° image sonar, and a USBL. Fig. 2 and Table 2 show the configuration and specifications of the ROV, respectively. The tilt camera and 360° image sonar are used to explore underwater structures or sea level, and the USBL is used to measure the relative position between the USV and ROV. The ROV is designed to have a weight of 17 kg and a negative buoyancy of 5.5 kg in water for easy depth control; it controls depth using the winch system and the depth sensor. With eight thrusters, it has six degrees of freedom in motion. The communication between the USV and ROV uses the TCP/IP method through the tether cable that allows underwater data to be checked in real time on land.

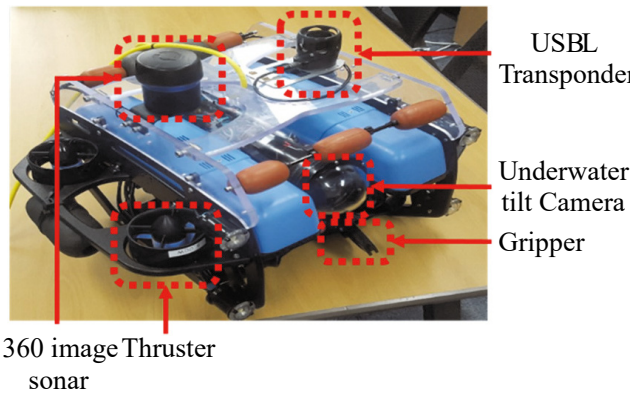

Fig. 2. Configuration of ROV

Table 2. Specifications of ROV

Size (L *W * H) (mm)	460*570*360
Weight (kg)	17
Main Controller	Pixhawk 1
Scanning Sonar	Ping 360
AHRS	AHRS mounted inside Pixhawk 1
Camera	Low-Light HD USB Camera
Depth sensor	BlueRobotics bar 100
Thruster	BlueRobotics T-200

3. System Structure of Complex Platform

The overall system configuration of the complex platform consists of a land-based operation console, an USV, a ROV, and a winch system connecting the USV and ROV. Fig. 3 shows the control configuration diagram of the controller, sensor, and actuator. The data is exchanged between the land-based operation console and USV through wireless TCP/IP equipment (AP Bridge), with a data transmission speed of approximately 80–90 Mbps that is sufficient to exchange FHD-class video data and 3D LiDAR data in real time. In addition, the battery capacity of the complex platform is selected so that USV and ROV can perform an 8-h mission at the same time.

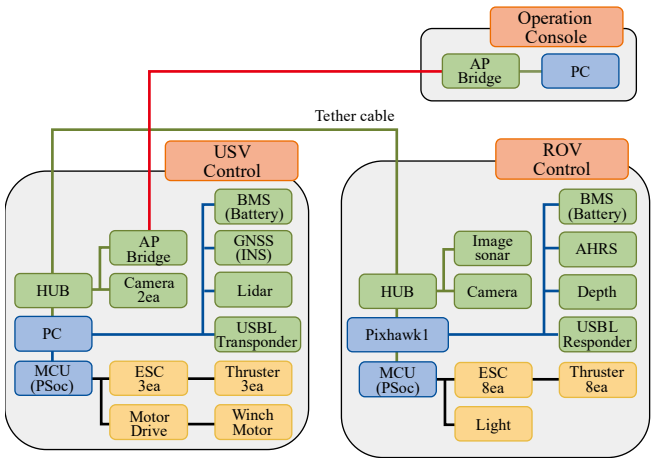

Fig. 3. Configuration diagram of complex system

4. Operating Program and Operation Console

The operating program is produced using C# and configured with a GUI so that the operator can easily check and control the information of each platform. Using this program, users can view the GPS location data of the USV, posture information of the AHRS, camera image data, and the relative location of the ROV through USBL data. In addition, by displaying the current location, heading angle, and autonomous route of the USV on the Google Map, the operator can intuitively see whether the USV is moving along the set route. The operating program can be operated either manually using a joystick or by programming to take autonomous navigation commands such as dynamic positioning (DP) and winch control.

The operation console is contained in a waterproof case and consists of PC components, a joystick, and inverters. The components of commercial desktop PCs are used to facilitate processing, maintenance, and repair of large amounts of incoming data in real time, and an AC-DC inverter is used to provide the necessary power to the AP Bridge and other components. Figs. 4 and 5 show the configuration of the operation program and operation console, respectively.

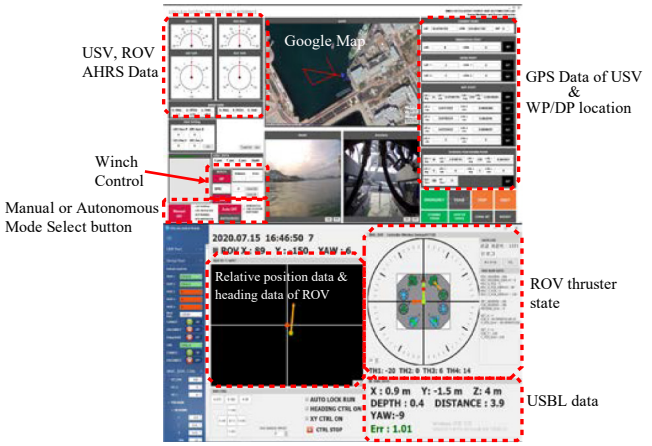

Fig. 4. Configuration of operation program

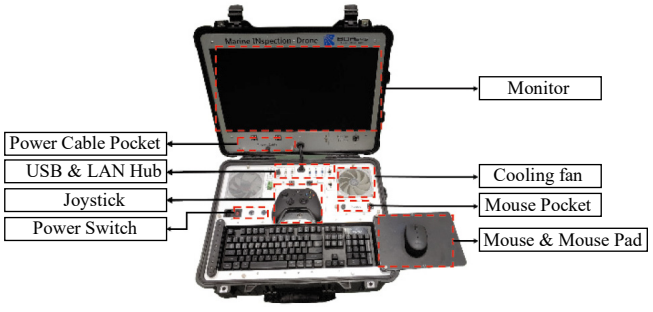

Fig. 5. Configuration of operation console

III. DYNAMICS AND CONTROL SYSTEM

1. Dynamics of Complex Platform

Fig. 6 and Table 3 shows the frame of the complex platform and outlines the coordinate system, respectively.

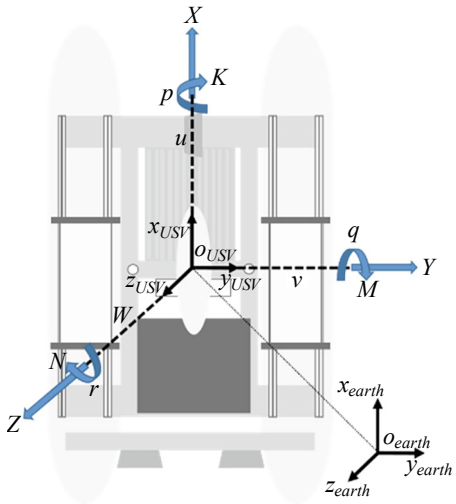

Fig. 6. Coordinates of complex platform

Table 3. Notation of SNAME for complex platform

	force and moments	linear and angular velocity	position and Euler angles
motions in the x direction (surge)	X	u	x
motions in the y direction (sway)	Y	v	y
motions in the z direction (heave)	Z	w	z
rotation about the x-axis (roll)	K	p	φ
rotation about the y-axis (pitch)	M	q	θ
rotation about the z-axis (yaw)	N	r	ψ

The basic formulas of dynamics are based on the Newton–Euler equations and vectorial-matrix dynamics. Because the USV moves in the x-axis and y-axis, it has three degrees of freedom and is capable of surge, sway, and yaw motions. The dynamic equations of the USV are expressed in (1a), (1b), and (1c).

$$\left(m-X_{(\dot{u})}\right)v\left(\dot{u}\right)-r+\left(Y_{(\dot{v})}vr+Y_{(\dot{r})}r-mx_G r\right)r -\left(X_u+X_{u|u|}|u|\right)u=\tau_x \tag{1a}$$

$$\left(m-Y_{(\dot{v})}\right)\left(\dot{v}\right)+\left(mx_G-Y_{(\dot{r})}\right)\left(\dot{r}\right)+r-X_{(\dot{u})}u_r r- \left(Y_v+Y_{v|v|}|v|\right)v-\left(Y_r+Y_{r|r|}|r|\right)r=\tau_Y \tag{1b}$$

$$\left(mx_G-N_{(\dot{v})}\right)\left(\dot{V}\right)+ \left(I_Z-N_{(\dot{r})}\right)\left(r-\left(Y_{(\dot{v})}v_r r-\dot{Y}_{(\dot{r})}r+mx_G r\right)u\right) +X_{(\dot{u})}u_r v-\left(N_v+N_{v|v|}|v|\right)-\left(N_r+N_{r|r|}|r|\right)r=\tau_N \tag{1c}$$

Here, τ represents the thrust force. Detailed definitions of related parameters and conditions are provided in the related studies (Fossen, 1994; Cho et al., 2020). The ROV motion has six degrees of freedom: surge, sway, heave, roll, pitch, and yaw. The heave of the ROV is achieved through winch control; therefore, the dynamic equation of the ROV is expressed as in (2a), (2b).

$$M_{RB}\dot{\nu}+M_A\nu_w+C_{RB}(\nu)\nu+C_A(\nu)\nu +D(\nu_w)\nu_w+g(\eta)=\tau \tag{2a}$$

$$\tau=\left[\tau_1\ \tau_2\ldots\tau_5\ \tau_6\right]^T \text{ where, } \tau_3=\tau_3'+\tau_w \tag{2b}$$

τ_3' means the thrusting force to heaving and τ_w means the winch force. The conditions and detailed definitions of related parameters can be found in related studies (Fossen, 1994; Wu and Eng, 2018).

2. Control System of Complex Platform

The control method of the complex platform is based on a proportional–integral–derivative (PID) controller. The USV and ROV are controlled to move to the target point, and the dynamic positioning (DP) control is applied to the USV to enable the ROV to perform underwater tasks. The controller also prevents the USV and ROV from deviating from the task point. Moreover, the parameter gain-tuning algorithm was developed for the PID control.

The propulsion control system of the USV consists of the bearing control and the surging control. The bearing control is the process of adjusting the heading angle of the hull to align with the target direction angle obtained using the line of sight (LOS), and the surging control is the process of adjusting the linear motion of the hull by considering the distance between the current position of the platform and the target point as an error.

This study applied a method not only considers the linear motion during the surging control, but also the rotational motion to account for the cross-track error of the platform. The PID-based controller for both linear and rotational directions is expressed in (3a) and (3b), respectively.

$$T_\psi=K_{P_\psi}e_\psi+K_{I_\psi}\int e_\psi+K_{D_\psi}(\dot{e}_\psi) \tag{3a}$$

$$T_d=K_{p_d}e_d+K_{I_d}\int e_d+K_{D_d}(\dot{e}_d) \tag{3b}$$

where T_ψ and T_d are the direction and distance output of the

controller, respectively, and e_ψ and e_d are the heading and distance errors, respectively.

3. Algorithm of Cross-track Error

The cross-track error (CTE) refers to a linear distance error caused by disturbances such as waves, wind, and tides in the target and actual moving paths of the platform. In this study, a new CTE method was proposed, whose simplified schematic diagram is shown in Fig. 7.

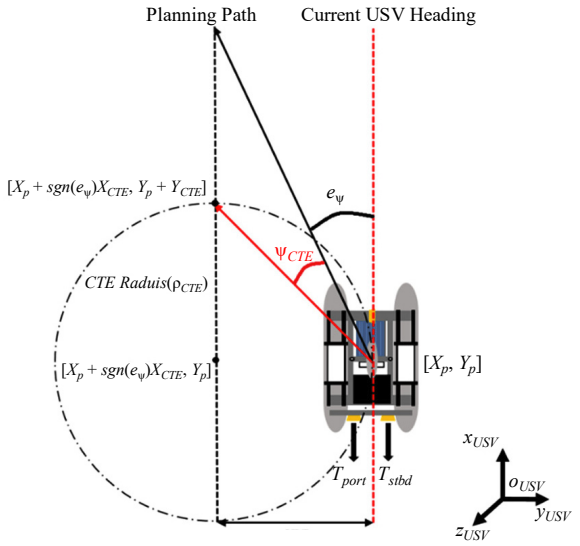

Fig. 7. Schematic of CTE

In this study, to reduce the CTE during the USV surging control, the center of the platform, $[X_p, Y_p]$ is moved by Y_{CTE} in the y-axis direction, resulting in new coordinates, $[X_p, Y_p + sgn(e_\psi)Y_{CTE}]$. Next, a circle ρ_{CTE} is drawn with the new point as the center point, and the new target direction angle, ψ_{CTE} is calculated using the forward contact, $[X_p + X_{CTE}, Y_p + sgn(e_\psi)X_{CTE}]$ as the target point between ρ_{CTE} and the target path. Subsequently, the calculated ψ_{CTE} is subtracted from the target direction angle e_ψ obtained using the LOS. The value of E_ψ obtained by subtracting e_ψ from ψ_{CTE} is used as an error in the PID control. Finally, the PID algorithm applied to the CTE is expressed in (4) as follows.

$$T_{CTE} = K_{P\psi}(E_\psi) + K_{I\psi}\int E_\psi + K_{D_\psi}(\dot{E}_\psi) \quad (4)$$

Where $E_\psi = e_\psi - \psi_{CTE}$

The output of the controller from the CTE algorithm is the propulsion force of the port side thruster or the starboard side thruster, depending on the sign of e_ψ. The output of each thruster is expressed in (5).

$$\begin{aligned} T_{Port} &= T_{CTE} \quad \text{if } e_\psi < 0 \\ T_{stbd} &= T_{CTE} \quad \text{if } e_\psi > 0 \end{aligned} \quad (5)$$

Fig. 8 shows the block diagram of the PID controller considering the CTE.

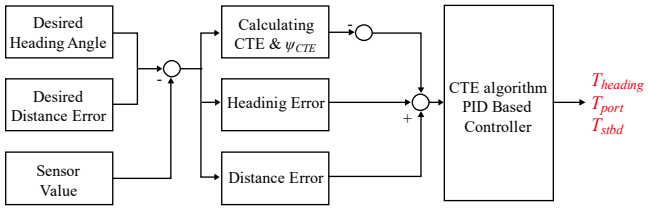

Fig. 8. Block-diagram of CTE algorithm

4. Dynamic Positioning Algorithm of USV

Dynamic positioning is an algorithm used to maintain a certain angle or position of the platform. The DP algorithm developed in this study is programmed to align the bow, which receives less drag, in the direction of tidal currents to reduce the influence of drag in the area with a high current. Subsequently, the GPS is used to detect the vehicle being pushed by the current, and the algorithm controls the bow direction to dynamically position it on the task position. The DP of the USV ensures that the USV and ROV remain in the task position. Fig. 9 shows the simplified schematic diagram of the DP algorithm used in this study.

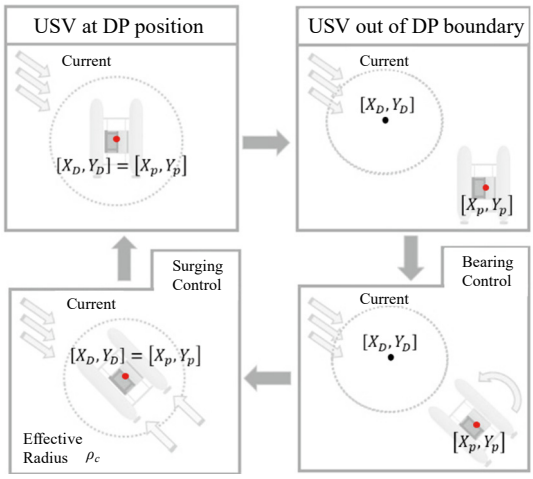

Fig. 9. Schematic of DP algorithm

The aim of the DP of the USV is to keep the distance error of the USV within the effective radius ρ_c using the propulsion control system and the CTE algorithm described above. This is expressed in (6) as follows:

$$\left[X_D\text{-}X_p\right]^2+\left[Y_D\text{-}Y_p\right]^2<\rho_c^2 \tag{6}$$

where X_D and Y_D represent the position of the target point, and X_p and Y_p represent the current position of the USV.

5. Sliding Mode Control of ROV

The dynamics of ROV under the water are described with 6 DOF, and its dynamics are well described in (Fossen, 1994). The translational motion control of the ROV was performed in a study (Cho et al., 2020) using the underwater position sensor, USBL. This study conducted the posture control required for hovering motion of the ROV. Hence, 3 DOF motion of ROV related with yaw, roll, and pitch angles with related disturbances such as uncertain hydrodynamic forces are described in Equation (7). To overcome such disturbances and achieve stable posture control of the ROV, the sliding mode control (SMC) was designed and applied in the actual experiment. The SMC was applied to achieve robust control of yaw, roll, and pitch. Here, the Coriolis added mass term and hydrodynamic damping are omitted due to their small values under the situation of slow hovering motion. The parameters can be found in related studies (Jacques and Slotine, 1990).

$$M\ddot{x}+C(x,\dot{x})+g(x)=u \tag{7}$$

Where

$$\dot{x}=\begin{bmatrix}p & q & r\end{bmatrix}^T,\ u=\begin{bmatrix}u_p & u_q & u_r\end{bmatrix}^T.$$

$$M=M_{RB}+M_A=\begin{bmatrix}I_x-K_{\dot{p}} & 0 & 0\\ 0 & I_y-M_{\dot{q}} & 0\\ 0 & 0 & I_z-N_{\dot{r}}\end{bmatrix},$$

$$C=\begin{bmatrix}(I_z-I_y)qr-(\dot{r}+pq)I_{xz}+(r^2-q^2)I_{yz}+(pr-\dot{q})I_{xy}\\ (I_x-I_z)rp-(\dot{p}+qr)I_{xy}+(p^2-r^2)I_{zx}+(qp-\dot{r})I_{yz}\\ (I_y-I_x)pq-(\dot{q}+rp)I_{yz}+(q^2-p^2)I_{xy}+(rq-\dot{p})I_{zx}\end{bmatrix},$$

$$g(x)=\begin{bmatrix}W_{z_g}\cos(\theta)\sin(\theta)\\ W_{z_g}\sin(\theta)\\ 0\end{bmatrix}$$

To control these 3 axes robustly, SMC was applied. When defining error as $\tilde{x}=x-x_d$, s and $\dot{s}$ are expressed in (8) and (9), respectively.

$$s=M\left(\frac{d}{dt}+\lambda\right)\tilde{x}=M(\dot{\tilde{x}}+\lambda\tilde{x},\quad \lambda)>0 \tag{8}$$

$$\dot{s}=M\left(\ddot{\tilde{x}}+\lambda\dot{\tilde{x}}\right)=u-C\dot{x}|\dot{x}|-g(x)-M(\ddot{x}_d-\lambda\dot{\tilde{x}}) \tag{9}$$

At this time, the Lyapunov function must be established. Therefore, λ is set to $\frac{1}{2}M\frac{d}{dt}s^2=M(\dot{s})s\le 0$.

Thus, the control inputs u and gain k are expressed in (10).

$$u=\hat{M}\left(\ddot{x}_d-\lambda\dot{\tilde{x}}\right)+\hat{C}\dot{x}|\dot{x}|+g(x)-k\,\mathrm{sgn}(s) \tag{10}$$

where

$$k>\left\|\left(\hat{M}-M\right)\left(\ddot{x}_d-\lambda\dot{\tilde{x}}\right)+\left(\tilde{C}-C\right)\dot{x}|\dot{x}|\right\| \tag{10}$$

Fig. 10 shows the block diagram of a PD controller and the SMC. In SMC controller, robust action ksgn(s) is added to PD control.

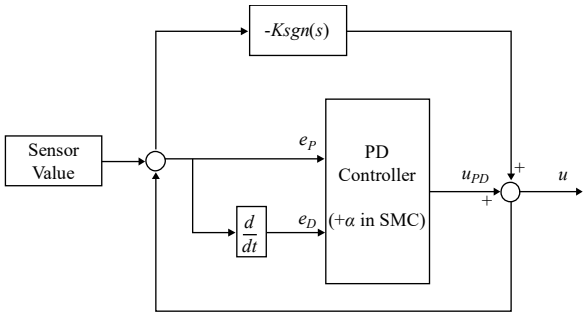

Fig. 10. Block diagram of SMC

IV. PERFORMANCE TEST OF COMPLEX PLATFORM

1. Performance Test of GNSS

The GNSS (Hemisphere Vector V113) sensor of the complex platform developed in this study is a type of sensor that displays both GPS data and heading data. Hence, performance tests for the GPS and the heading of the GNSS sensor were performed in parallel.

The GPS performance test and the heading performance test were conducted at a point [35.0745977, 129.0858546] inside the Korea Maritime and Ocean University, and the heading of the GNSS was set at 330°. The experiment was conducted for about an hour, and periodic vibration was applied during the experiment to mimic rolling and pitching that usually occur when the USV is in operation. The results of each test are shown in Figs. 11 and 12.

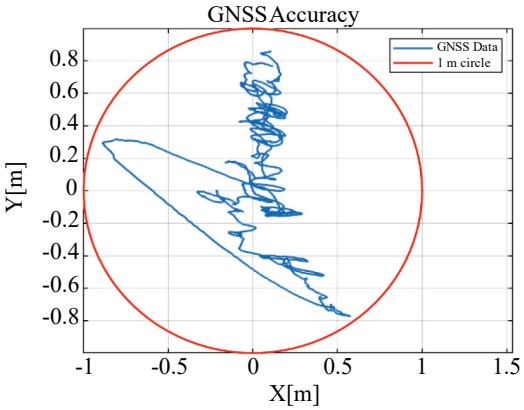

Fig. 11. Result of GPS performance test

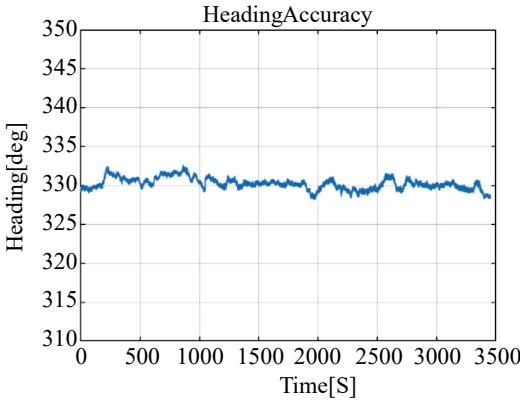

Fig. 12. Result of heading performance test

2. Performance Test of USBL

The USBL (SeaTrac X150, X010) performance test was conducted off the shore of the Korea Maritime and Ocean University. The experiment was conducted by attaching a USBL transponder to a structure with a length of 5.4 m and a depth of 1 m, and matching the true north and USBL heading direction. A USBL responder was attached to a structure with a length of 2 m and a depth of 2 m. Fig. 13 shows the simplified schematic of the coordinate system and experimental method used in the study.

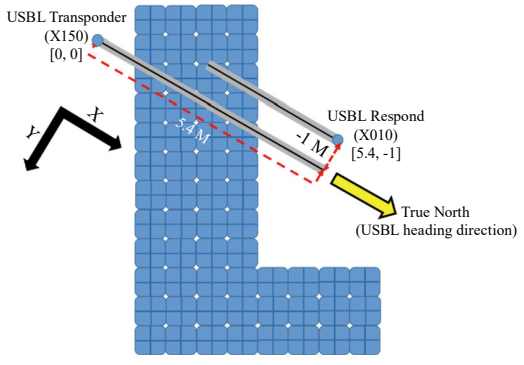

Fig. 13. USBL test in sea

In the experiment, the x-axis was set along the true north and the USBL transponder position was set at [0, 0]. The USBL responder was placed at coordinates [5.4, –1]. During the experiment, 255 heading and 103 position data were collected. The mean yaw value of the USBL was 0.7724° that had an error of 0.7°, and the mean position values were [5.3398, –0.9019] that had an error of approximately 6 cm in the x-axis direction and approximately 10 cm in the y-axis direction. The results of the USBL performance experiment are shown in Fig. 14.

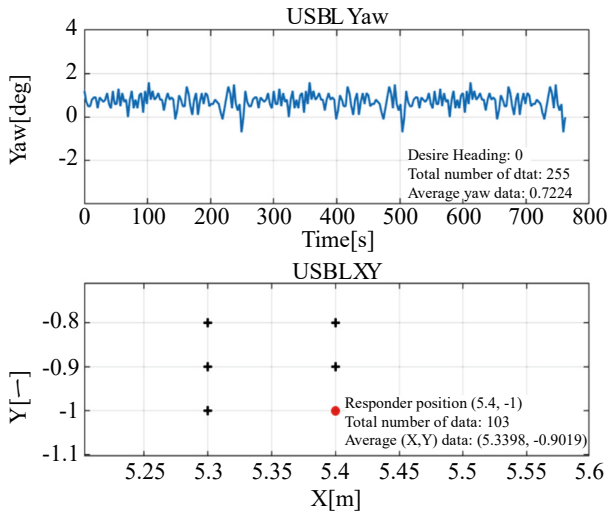

Fig. 14. Result of USBL performance test

3. DP Performance Test of USV at Sea

Prior to the real sea test of the complex platform, DP test was conducted to verify the DP performance of the USV. The experiment was conducted offshore of the Korea Maritime and Ocean University. The DP test was performed for 250 s with the USV at a point [35.07191488, 129.0854151] within the experimental area and a target point [35.0750216, 129.0849246] approximately 45 m away from the original point. Fig. 15. shows the USV during the DP performance test.

Fig. 15. USV during DP performance test

The effective DP radius ρ_c of the USV was set to 3 m for the test. The DP performance test results are shown in Fig. 16.

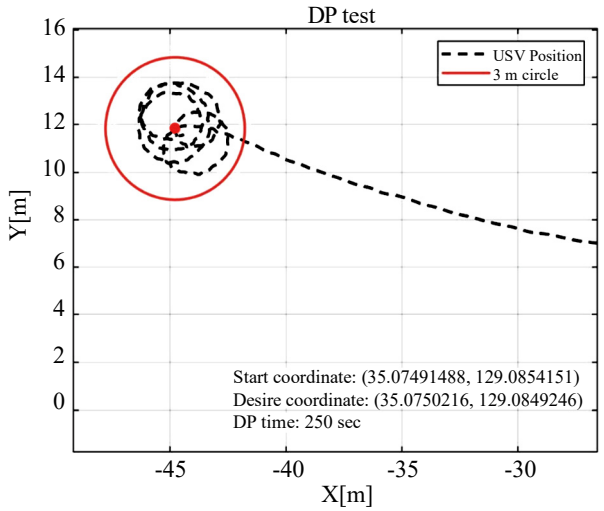

Fig. 16. Result of USV DP performance test

4. DP Performance Test of Complex Platform at Sea

The real sea test of the complex platform was conducted at the same location where the USV DP performance test was conducted, as described in the previous section.

The DP performance test of the complex platform was conducted by dynamic positioning of the USV at the same coordinates [35.0750216, 129.0849246] for 10 min and setting the DP of the ROV as [0, 0]. Considering that the ROV may affect the USV during DP, the effective radius ρ_c of the USV DP was changed from 3 m to 4 m. From 433 data points collected, it was confirmed that the USV DP was within an effective radius of 4 m and the ROV had an error of about 40 cm in the x-axis direction and approximately 50 cm in the y-axis direction, with a mean value of [–0.4095 m, –0.5348 m]. Figs. 17 and 18 show the results of the DP performance test of the complex platform.

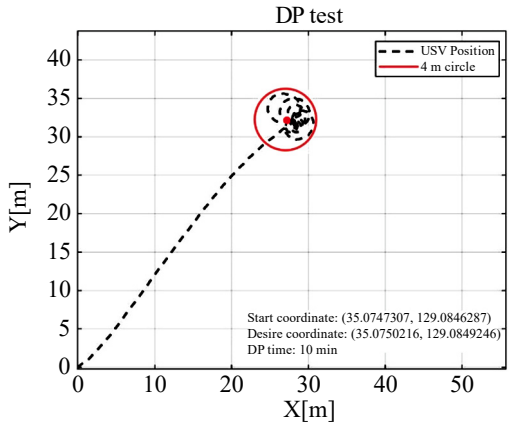

Fig. 17. Result of complex platform (USV) DP performance test

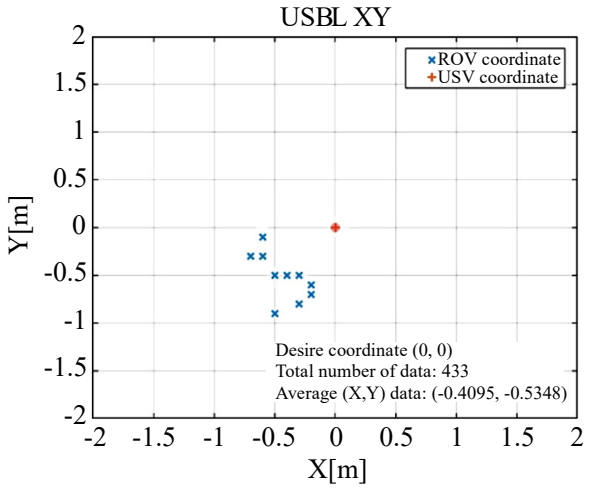

Fig. 18. Result of complex platform (ROV) DP performance test

5. Performance Test of ROV Hovering Control at Sea

In this study, the USV was used to move the ROV to the task position for exploration. At the task position, the USV performed DP, and the ROV hovered at the task position. This study used a PD controller, a commonly used device for ROV posture control in water, and the SMC that robustly offsets the effect of disturbances in water. The performances of the PD controller and SMC were compared. A gyro sensor was used as the posture sensor. In the experiment, the USV underwent DP at a point (35.07191488, 129.0854151) in the experimental sea area. After the ROV control was established using the PD controller, the SMC, including the robust control item that eliminates disturbances at the same PD gain, was tested. The control experiment was conducted for approximately 1 min under almost identical conditions. The data measurement interval was 0.1 s, and the target angles for roll, pitch, and yaw were 0°, 0°, and 50°, respectively. Figs. 19–21 show the results of the stability tests for roll, pitch, and yaw, respectively. The results show that the SMC exhibits superior performance and less error compared to the PD control. In Table 4 the RMS control error results of PD and SMC are presented. According to the test results in Table 4, the robust SMC showed better performance than PID control for roll, pitch, and yaw angle control of the ROV by 21%, 33%, and 30%, respectively.

Table 4. Comparison between the PD and SMC results

Angle	PD error	SMC error
Roll	–0.77940	–0.61474
Pitch	0.59657	0.39623
Yaw	–0.42525	–0.29591

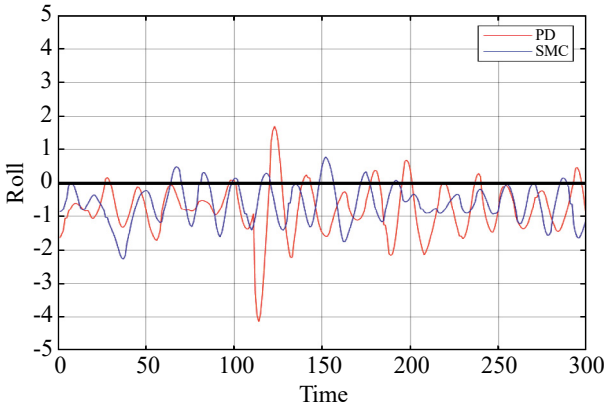

Fig. 19. Roll test of ROV applying PD and SMC

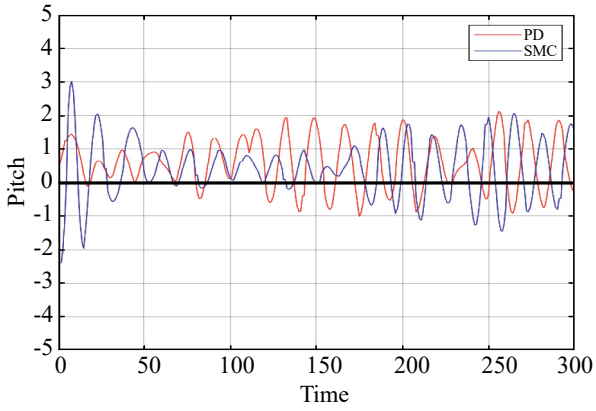

Fig. 20. Pitch test of ROV applying PD and SMC

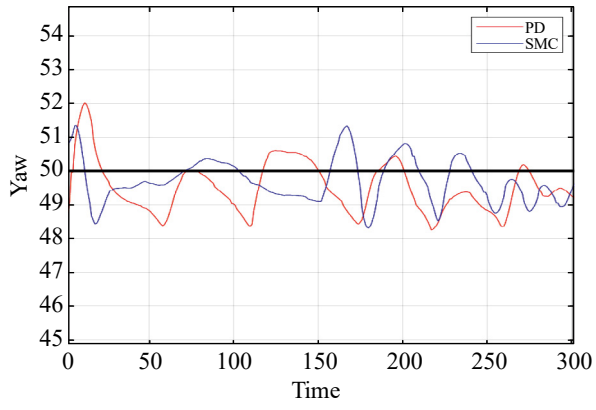

Fig. 21. Yaw test of ROV applying PD and SMC

V. CONCLUSION

The present study used a USV with high operability and an ROV capable of performing underwater tasks for the research and development of a complex platform that provides stable power supply and real-time acquisition of underwater data. The developed complex platform is intended to provide long-term operation, real-time data and control, and precise relative position measurement using GPS and USBL. Subsequently, the structure and control system of the complex platform consisting of a USV, an ROV, and a winch system were designed and manufactured, and an integrated control algorithm was developed.

The performance of the developed complex platform was verified through real sea experiments. In particular, for the surging control, a new CTE algorithm was proposed and used in sea experiments. Furthermore, the sensor performance tests were conducted to ensure the performance of the actual platform and to validate the acquired sensor data. For the DP test of the USV, the effective DP radius condition was set to 3 m, and the test result showed that the DP control satisfied the condition. For the performance test of the ROV hovering control at sea, the PID and robust SMC were applied. The robust SMC showed better performance than PID control in roll, pitch, and yaw angle control of the ROV by 21%, 33%, and 30%, respectively.

REFERENCES

Bentley, R. W. (2002). Global oil & gas depletion. Proceeding of Energy policy 30(3), 189–205.

BORSYS. (2019). Technology Transfer Commercialization on the Development of Combined marine Drones for High Precision Inspection of Underwater Pipes and Cables Proceeding of Korea Ministry of Science and ICT, Sejong, Korea; National Research Foundation of Korea, Daejeon, Korea.

Chen, Y., Y. Liu, Y. Meng, S. Yu and Y. Zhuang (2019). System modeling and simulation of an unmanned aerial underwater vehicle. Proceeding of J. Mar. Sci. Eng 7, 444.

Cho, H., S. K. Jeong, D. H. Ji, N. H. Tran, M. Vu and H. S. Choi (2020). Study on control system of integrated unmanned surface vehicle and underwater vehicle. Proceeding of Sensors 20, 2633.

Chu-Jou Wu, B. Eng. (2018). 6-DoF Modelling and Control of a Remotely Operated Vehicle. Proceeding of Flinders University, Adelaide, South Australia.".

Fossen, T. I. (2011). Handbook of marine craft hydrodynamics and motion control. Proceeding of John Wiley & Sons: Hoboken, NJ, USA.

Jacquees, J. and E. Slotine (1990). Applied nonlinear control. Proceeding of Massachusetts Institute of Technology, BT, USA.

Kim, T. S., C. H. Kim and M. K. Lee (2015). Study on the design and the control of an underwater construction robot for port construction. Proceeding of Journal of Navigation & Port Research 39(3), 253–260.

Lachaud, E., Y. Monbeig, P. Nolleau, A. Hardy, M. Thompson and M. Lardeux (2018). Opportunities and challenges of remote operating a ROV embarked on a USV. Proceeding of the Offshore Technology Conference, Houston, TX, USA, 30.

Lyu, B., Z. Zeng, D. Lu, L. Lian, J. Tu, L. Xiao and Y. Liu (2018). Combined small-sized USV and ROV observation system for long-term, large-scale, spatially explicit aquatic monitoring. Proceeding of the 2018 OCEANS-MTS/IEEE Kobe Techno-Oceans (OTO).

Molland, A. F., J. F. Wellicome and P. R. Couser (1994). Resistance experiments on a systematic series of high speed displacement catamaran form: variation of length-displacement ratio and breadth-draught ratio. Proceeding of Ship Science Report, 71.

Nicholson, J. W. and A. J Healey, (2008). The present state of autonomous underwater vehicle (AUV) applications and technologies. Proceeding of Marine Technology Society Journal 42(1), 44-51.

Rodriguez, J., H. Castaneda and J. L. Gordillo (2019). Design of an adaptive sliding mode control for a micro-AUV subject to water currents and parametric uncertainties. Proceeding of J. Mar. Sci. Eng 7, 445.

USV CAT-Surveyor. (2020). Available online: https://www.subsea-tech.com/cat-surveyor/ (accessed on 10 April).

Vu, M., H. S. Choi, J. K. Kang, D. H. Ji and S. K. Jeong (2017). A study on hovering motion of the underwater vehicle with umbilical cable. Proceeding of Ocean Engineering 135, 137–157.

Vu, M., M. Van, D. H. P. Bui, Q. T. Do, T.-T., Lee, S.-D. and H.-S. Choi (2020). Study on dynamic behavior of unmanned surface vehicle-linked unmanned underwater vehicle system for underwater exploration. Proceeding of Sensor 20, 1329.

ACKNOWLEDGMENT

This research was supported by “Data Collection System with Underwater Glider (19AR0001)” funded by Agency for Defense Development, Korea.